Title
THE ELECTRONIC STRUCTURE OF PbSe AMD PbTe II. OPTICAL PROPERTIES

Authors
Martinez, G.
Schluter, M.
Cohen, Marvin L.

Publication Date
1974-11-01

Submitted to Physical Review

LBL-3537
Preprint

THE ELECTRONIC STRUCTURE OF PbSe AND PbTe
II. OPTICAL PROPERTIES

G. Martinez, M. Schluter and Marvin L. Cohen

November, 1974

Prepared for the U. S. Atomic Energy Commission
under Contract W-7405-ENG-48

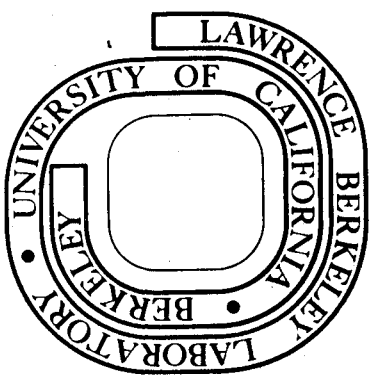

DISCLAIMER

The Electronic Structure of PbSe and PbTe*

II. Optical Properties

G. Martinez†, M. Schlüter‡ and Marvin L. Cohen
Department of Physics, University of California and
Inorganic Materials Research Division,
Lawrence Berkeley Laboratory, Berkeley, California 94720

Abstract

We present calculations related to the optical properties of PbSe and PbTe in an energy range from 0 to 26 eV based on recently developed band-structure models. The results are compared to measurements of the low energy real part of the refractive index, to modulated reflectivity measurements for energies up to 6 eV, to energy loss experiments for energies up to 20 eV and to synchrotron radiation reflectivity measurements involving transition from core d-levels. The agreement between the experimental data and theory can in some cases be improved by using OPW functions in calculating transition matrix elements. Differences between synchrotron radiation reflectivity measurements and photoemission data are analyzed and discussed.

I. Introduction

In a previous paper[1] we have presented models for the band structures of PbSe and PbTe based on the empirical

pseudopotential method (EPM). As shown in this paper, the EPM scheme had to be improved by the introduction of an effective mass and a fully non-local d-like potential. We have also shown that the band structures obtained in this way reproduce quite well the band edge effective masses, the Knight shift experiments and the UPS and XPS photo-emissions results for both compounds. In this paper we shall compare the results of optical experiments to calculations of the optical constants. The experimental data, reflectivity and modulated reflectivity are now available over a range of about 28 eV. Thus comparing our models to these measurements over this range of energy can be considered as a very good test of the validity of our band structures.

In section I we present the procedure to calculate the imaginary part of the frequency dependent dielectric function $\varepsilon_2(\omega)$, as well as the real part $\varepsilon_1(\omega)$ for normal EPM calculations and for a model in which the dipole matrix elements are evaluated using wave functions which are orthogonalized to the core wave functions. In section III we compare our results to wavelength modulated reflectivity between 2 and 6 eV. Section IV will contain a discussion of all the optical spectra for valence- to conduction band transitions in the range from 0 to 18 eV. In section V we compare new optical reflectivity measurements for transitions from lead d core levels into conduction states with the results of our calculations.

II. Derivation of the dielectric function

The imaginary part of the transverse dielectric function for $q = 0$ is given by

$$\varepsilon_2(\omega) = \frac{4\pi^2 e^2 \hbar}{3m^2\omega^2} \sum_{c,v} \int_{BZ} \frac{2}{(2\pi)^3} \delta(\omega_{c,v}(\underset{\sim}{k})-\omega)|M|^2 d^3\underset{\sim}{k} \quad (1)$$

where c,v are the band indices for conduction- and valence bands, $|M|^2$ is the absolute squared dipole matrix element between these bands, and $\hbar\omega_{c,v}$ is the energy separation between them. Once $\varepsilon_2(\omega)$ is known, $\varepsilon_1(\omega)$, the real part of the dielectric function, can be calculated by means of a Kramers-Kronig transformation, assuming a reasonable analytical tail function for $\varepsilon_2(\omega)$ at very high frequencies. Knowing $\varepsilon_1(\omega)$ and $\varepsilon_2(\omega)$ optical data such as reflectivity and its derivative can easily be calculated. To evaluate Eq. (1) we need to know the band structure and the transition matrix elements at a large number of $\underset{\sim}{k}$-points in the irreducible part of the Brillouin zone. The $\underset{\sim}{k}$-space integration has been done using the scheme developed by Gilat and Dolling,[2] which consists of dividing the irreducible part of the Brilluoin zone (1/48) into a mesh of small cubes. In each cube, we calculate $\omega_{c,v}$ for all c and v, the corresponding $|M|^2$ and the gradient of the energies $\omega_{c,v}$ with respect to $\underset{\sim}{k}$ which is necessary for an interpolation procedure between each cube. All matrix elements and energy gradients are calculated in a $\underset{\sim}{k}\cdot\underset{\sim}{p}$ scheme. The use of pseudo-wavefunctions instead of orthogonalized wavefunctions is

believed to cause only small errors in the integration scheme. However, the process of orthogonalization can have remarkable effects on the transition matrix elements. This has already been encountered in calculating core- to conduction band transitions[3] for valence- to conduction band transitions. This effect is smaller in the usual optical constant calculations but it can still be important, e.g. for reproducing the exact absolute value of the index of refraction (or $\sqrt{\varepsilon_1(0)}$) at zero frequency. It is therefore interesting to calculate the optical constants in both ways with and without orthogonalized wavefunctions and to demonstrate the effect of orthogonalization. The orthogonalized wavefunction $\psi_{\underset{\sim}{k}}(r)$ can be expressed in terms of pseudo wavefunctions $\phi_k(r)$ and core wavefunctions $b_t{}^{\alpha}$ as:

$$|\psi_{\underset{\sim}{k}}(\underset{\sim}{r})> = |\phi_{\underset{\sim}{k}}(\underset{\sim}{r})> - \sum_{t,\alpha} <b_t{}^{\alpha}|\phi_{\underset{\sim}{k}}(\underset{\sim}{r})>|b_t{}^{\alpha}> \qquad (2)$$

Here $|b_t{}^{\alpha}>$ is any core (t) wavefunction corresponding to any atom α; it can be written as:

$$|b_t{}^{\alpha}> = \frac{1}{\sqrt{N}} \sum_{\nu,\alpha} e^{i\underset{\sim}{k}\cdot(\underset{\sim}{R}_\nu+\underset{\sim}{\tau}_\alpha)} a_t(\underset{\sim}{r}-\underset{\sim}{R}_\nu-\underset{\sim}{\tau}_\alpha) \qquad (3)$$

where a_t stands for a core orbital, $\underset{\sim}{R}_\nu$ is a translation vector and $\underset{\sim}{\tau}_\alpha$ describes the position of atom α in the primitive cell. N is the number of cells in the crystal. We first require that the new wavefunction be normalized which leads to the following

$$<\psi_{\underset{\sim}{k}}(\underset{\sim}{r})|\psi_{\underset{\sim}{k}}(\underset{\sim}{r})> = 1 - \sum_{t,\alpha} |<b_t{}^{\alpha}|\phi_{\underset{\sim}{k}}(\underset{\sim}{r})>|^2 \qquad (4)$$

Furthermore, the optical dipole matrix element between a valence band v and a conduction band c is given by:

$$\langle\psi^v|\underset{\sim}{p}|\psi^c\rangle = \langle\phi^v|\underset{\sim}{p}|\phi^c\rangle - \sum_{t,\alpha} \langle\phi^v|b_t^\alpha\rangle\langle b_t^\alpha|\underset{\sim}{p}|\phi^c\rangle$$

$$- \sum_{t,\alpha} \langle\phi^v|\underset{\sim}{p}|b_t^\alpha\rangle\langle b_t^\alpha|\phi^c\rangle$$

$$+ \sum_{t,t',\alpha,\alpha'} \langle\phi^v|b_t^\alpha\rangle\langle b_t^\alpha|\underset{\sim}{p}|b_{t'}^{\alpha'}\rangle\langle b_{t'}^{\alpha'}|\phi^c\rangle \qquad (5)$$

where the first term on the right hand side is the usual pseudo matrix element for the optical transition. Assuming negligible overlapping between the core wavefunctions centered at different atoms, we can rewrite Eq. (5) as:

$$\langle\psi^v|\underset{\sim}{p}|\psi^c\rangle = \langle\phi^v|\underset{\sim}{p}|\phi^c\rangle - \sum_{t,\alpha} [\langle\phi^v|b_t^\alpha\rangle\langle b_t^\alpha|\underset{\sim}{p}|\phi^c\rangle$$

$$+ \langle\phi^v|\underset{\sim}{p}|b_t^\alpha\rangle\langle b_t^\alpha|\phi^c\rangle - \sum_{t'\neq t} \langle\phi^v|b_t^\alpha\rangle\langle b_t^\alpha|\underset{\sim}{p}|b_{t'}^{\alpha}\rangle\langle b_{t'}^{\alpha}|\phi^c\rangle] \qquad (6)$$

The pseudo wavefunction is expanded in plane waves,

$$|\phi_{\underset{\sim}{k}}^j(\underset{\sim}{r})\rangle = \frac{1}{\sqrt{\Omega}} \sum_{\underset{\sim}{G}} a_{\underset{\sim}{G}}^j(\underset{\sim}{k}) e^{i\underset{\sim}{K}\cdot\underset{\sim}{r}} = \sum_{\underset{\sim}{G}} a_{\underset{\sim}{G}}^j(\underset{\sim}{k})|\underset{\sim}{K}\rangle \qquad (7)$$

where $\underset{\sim}{K} = \underset{\sim}{k}+\underset{\sim}{G}$ and Ω is the volume of the crystal. To evaluate expression (4) and (5) we need to calculate the overlapping integrals $\langle b_t^\alpha|\underset{\sim}{K}\rangle$. These integrals are of the same kind as those needed in paper I to express the spin-orbit interaction or the non-local potential in the Hamiltonian. As we showed in that paper, it is reasonable to consider only those contributions t coming from the outermost core shell of each atom. Furthermore we shall

assume that the core wavefunctions are well represented by atomic orbitals[4] and that $a_t(r)$ in Eq. (3) can be written as:

$$a_t(\underset{\sim}{r}) = \sum_m C^t_{\ell m} R_\ell{}^n(r) Y_\ell{}^m(\theta,\phi) \qquad (8)$$

where t describes the set of quantum numbers (n,j,j_z) and the coefficients $C^t_{\ell m}$ are spinors. We find

$$\langle b_t{}^\alpha | \underset{\sim}{K} \rangle = \frac{4\pi}{\sqrt{\Omega_0}}(2\ell+1) i^\ell S^\alpha(\underset{\sim}{G})\left[\sum_m C^t_{\ell m} {}^* Y_\ell{}^{m*}(\hat{\underset{\sim}{K}})\right] \int_0^\infty dr\, r^2 R_\ell{}^n(r) j_\ell(K\cdot r) \qquad (9)$$

and similarly

$$\langle b_t{}^\alpha | p | \underset{\sim}{K} \rangle = \frac{4\pi}{\sqrt{\Omega}}(2\ell+1) K S^\alpha(\underset{\sim}{G})\left[\sum_m C^t_{\ell m} {}^* Y_\ell{}^{m*}(\hat{\underset{\sim}{K}})\right] \int_0^\infty dr\, r^2 R_\ell{}^n(r) j_\ell(K\cdot r) \qquad (10)$$

where Ω_0 is the volume of the unit cell, $j_\ell(K\cdot r)$ the spherical Bessel function of order ℓ and $S^\alpha(\underset{\sim}{G})$ the structure factor for the atom α. Finally it is necessary to calculate the matrix elements $\langle b_t{}^\alpha | \underset{\sim}{p} | b_{t'}{}^\alpha \rangle$ in (5). This was done by use of the standard selection rules of atomic dipole transitions and by use of atomic wavefunctions given by Hermann Skillmann.[4] The result is that the orthogonalization procedure leads to a general increase of the momentum matrix elements. This increase is about 10 to 20% for the square of the matrix elements at low energy (between 0 and 5 eV) and smaller for higher energies. The effect of this on the optical properties will be discussed below. We shall also need to interpret reflectivity measurements including transitions from 5d-level core states to conduction bands (see section V). This

involves calculating matrix elements of the form $\langle b_{5d}{}^{i}|\underset{\sim}{p}|\psi^{c}\rangle$ which can in the same fashion as in (5) be written as

$$\langle b_{5d}{}^{j}|\underset{\sim}{p}|\psi^{c}\rangle = \langle b_{5d}{}^{j}|\underset{\sim}{p}|\phi^{c}\rangle - \sum_{t}\langle b_{5d}{}^{j}|\underset{\sim}{p}|b_{t}\rangle\langle b_{t}|\phi^{c}\rangle \qquad (11)$$

where the summation over t is restricted due to selection rules to 5p lead core levels. In this case the square of the matrix elements using orthogonalized wavefunctions is an order of magnitude larger than those computed with pseudo wavefunctions,[3] which demonstrates the necessity for the orthogonalization correction in this case.

III. Modulated reflectivity

In this energy range a large number of experiments like room temperature reflectivity measurements[5] are available. More recently modulated reflectivity measurements[6] have been performed in this energy range. Because of the precision and because they have been obtained at helium temperatures the modulated spectra are useful for comparison with the calculated spectra. This comparison is shown in Fig. 1 for PbTe and PbSe. The quantitative comparison is made in Table I where we also assigned the different structures to transitions at critical points in k-space. To facilitate the discussion of these assignments, we have reproduced in Fig. 2 the band structure of PbTe as derived in paper I. This band structure (in the present context) can be assumed to be typical for both lead salts. The position of the peaks in ε_2 or in the reflectivity do <u>not</u> depend on the kind of matrix elements --

with or without orthogonalization -- we used for the calculation. The assignments show that the two main peaks in ε_2, located at 2.2 eV for PbTe and at 3.2 eV for PbTe, are due to several transitions. Among them the most important transitions come from a region in k-space around the point p with the coordinates (0.625, 0.46, 0). This "volume effect" has already been found for the E_2 peak of germanium[10] and it is probably a general feature for most of the semiconductors. It is worth noting that this point p is not far away from the "Baldereschi" point[11] $\underset{\sim}{k}$ = (0.6223,0.2953,0) for face centered cubic crystals.

IV. Optical properties for energies lower than 18 eV

All transitions described in the previous chapter fall in this energy range. In addition, after 6 eV we enter a range in which transitions into d-conduction bands occur. The onset of these transitions corresponds to the transition at χ(5-6) at 5.9 eV for PbTe and at 6.3 eV for PbSe. We see in Table I that all the high energy transitions involve extended regions in k-space which follows from the fact that the oscillator strength for different transitions is decreasing rapidly and becoming approximately equal for large areas in k-space above an energy of the order of 6 to 7 eV. We also see from Table I that the main structures in this range are generally reproduced correctly.

In Figure 3 (PbTe) and in Figure 4 (PbSe) we show the imaginary part of the dielectric function $\varepsilon_2(\omega)$ calculated

using pseudo matrix elements and using OPW matrix elements. As already mentioned, the use of OPW matrix elements significantly increases the imaginary part of the dielectric function in the low energy range ($\lesssim$ 6eV). We have also presented in these figures the reflectivity spectra calculated with the OPW matrix elements; these are compared in the range of 2 to 6 eV to experimental data.[6] For this quantity the corresponding curve obtained with the use of pseudo matrix elements is only a little lower for the whole energy range and has not been reproduced here. A problem arises when we try to compare the absolute values of the reflectivity with those found experimentally at high energies. Typically it is found[5] that at 12 eV the reflectivity (at 300°K) should have a magnitude between 0.12 and 0.16. We there calculated a reflectivity of at least 0.25 whereas at lower energies the agreement between theory and experiment is very good. This discrepancy is quite difficult to explain. As far as temperature effects are concerned it would be difficult to understand why the temperature would influence the reflectivity at high energies and not at low energies. On the other hand we might think about the influence of local field effects on the dielectric function. A simple approximate way to include them would be to use a classical Lorentz-Lorenz relation as it has been done by Bergstresser and Rubloff.[12] This procedure is claimed to lead to a decrease of the reflectivity at higher energies, provided

at least one of the levels involved in the transition is fairly localized. This however seems not to be justified in our case, as seen from Table I since only the lower two s-bands are fairly localized states. The approach made by the authors in Ref. 12 is thus conceptually not valid in our case. That does not necessarily mean that a more sophisticated theory of local field effects in the dielectric function would not be appropriate in this range of energy and would not improve the agreement between theoretical and experimental results. Some doubt also remains concerning the absolute value of the reflectivity measurements at high energies in general. At these energies the diffusion on the surface might be important. An indication of this effect is available when comparing the energy of the plasmon energy derived from reflectivity measurements,[5] to the energy found directly[13] from electron loss experiments; the plasmon energy derived from reflectivity is about 3 eV lower than the energy found by electron loss experiments. This seems to indicate that the experimental reflectivity falls off too fast for higher energies.

Whereas the introduction of OPW matrix elements did not change the energies of the peaks in $\varepsilon_2(\omega)$ and in the reflectivity, this is no longer the case for the peaks in the imaginary part of $1/\varepsilon$. It has been shown[14] that electron loss experiments directly measure $\mathrm{Im}(1/\varepsilon)$. The peaks in the $\mathrm{Im}(1/\varepsilon)$ correspond to excitation of longitudinal

collective excitations of electrons of a given kind and occur when the sum rule involving the optical matrix elements is quasi exhausted[15] (or $\varepsilon_1(\omega)$ is going through 0 with a positive slope). As shown in Figures 5 and 6 for PbSe and PbTe we find a shift of the peak energies in the $\mathrm{Im}(1/\varepsilon)$ toward higher energies when using the OPW matrix elements instead of pseudo matrix elements. In these figures we have also included the energy range (18 eV to 30 eV) corresponding to transitions from 5d lead core-levels which shall be discussed in section V. The quantitative comparison with experiment is given in Table II. We see that the use of OPW matrix elements improves the agreement between theory and experiment. The appearance of the first peak in $\mathrm{Im}(1/\varepsilon)$ at ~6 eV before the main plasmon peak at ~15 eV is typical for ionic compounds. This peak originates from the existence in the band structure of a "quasi-optical gap" due to forbidden transitions rather than due to a zero joint density of states. Details of this question will be discussed in a later publication.[16] A second peak at about 9.7 eV for PbTe and 11 eV for PbSe is not clearly resolved by our band structure calculation. It should originate from the exhaustion of transitions starting from the lead s valence level. This peak is also characteristic for ionic compounds. The position of the main plasmon peak at about 15.5 eV is somewhat sensitive to the cut off of $\varepsilon_2(\omega)$ we used in our calculations. The curves presented here are obtained by cutting the valence

to conduction band transitions at 17 eV and replacing them by a tail function which varies like the imaginary part of the dielectric function for a plasmon ($\sim 1/\omega^3$).

A critical measure for the quality of the present band structures is obtained by comparing the experimental[17,18] and calculated low energy index of refraction. This is done in Figure 7 for PbSe and PbTe. The discrepancies between the energies at which the peaks occur are due to temperature effects on the gap and (or) to Burstein shifts arising from the doping of the thin layers used in the experiments. Therefore only the absolute values of the index of refraction are interesting for comparison. It follows from the figure that it is important to use the OPW matrix elements for a fairly accurate reproduction of the experimental results for the absolute value of the index of refraction. Other interesting information can be deduced from Figure 7. The jump of the index of refraction between zero energy and gap energy is about 0.6 for PbTe and 0.3 for PbSe; this is very well reproduced by our calculations. This jump is to first order proportional to the square of the matrix elements involved in transitions at the fundamental gap. Its difference by a factor of two indicates that the transition matrix elements at the gap are twice as important for PbTe than for PbSe. This is an indirect confirmation of the different band ordering we have chosen for the conduction bands of PbTe and PbSe (see paper I) since the band inversion is

the only possible way to explain such a difference in the magnitude of matrix elements.

V. Optical properties in the energy range from 18 to 26 eV

Recent experiments[3,19] using synchrotron radiation gave for the first time detailed information on transitions with energies over 18 eV. In this range we expect to see primarily transitions from the cation core-d levels into conduction states. Since the core levels retain their atomic-like character in the solid, i.e. they are essentially dispersionless, these transitions add new important information about the nature of conduction band states. Depending upon the angular momentum character of the core level, the core-conduction band transitions "filter out" specific angular momentum states of the conduction bands. In particular, if the initial state is a d-like core state and if the f-character of the conduction band is small or non-existent, then we obtain from reflectivity measurements the density of p-states in the conduction bands weighted by transition matrix elements.

To perform the calculations of $\varepsilon_2(\omega)$ involving transitions from core d-states we used OPW matrix elements, as derived in Eq. 9. As already mentioned in section II, the transition matrix elements calculated this way exceed the "pseudo" matrix elements by a factor of 3 to 4 and the contribution to $\varepsilon_2(\omega)$ arising from such transitions is an order of magnitude larger than that arising from valence-band to

conduction-bands transitions. We can therefore safely assume that all structures appearing in this energy range are due to transitions from d core lead levels into conduction bands. The total value of $\varepsilon_2(\omega)$ is then obtained by adding to this contribution a background decreasing like $1/\omega^3$ whose absolute value and slope are matched to the small interband $\varepsilon_2(\omega)$ at 18 eV. $\varepsilon_1(\omega)$ is obtained by a Kramers-Kronig analysis of $\varepsilon_2(\omega)$ over the full range of energies (0 to 40 eV). In figures 8 and 9 we compare the calculated reflectivity with the experimental spectra taken on PbSe and PbTe. The theoretical and experimental spectra are aligned at the transition threshold energies. The following discussion of the spectra holds qualitatively for both lead salts. We saw in paper I, that in agreement with Knight shift[20] experiments in both compounds the conduction band at L is dominated by Pb states having $6p^{42}$ character. Transitions from the highest core d levels ($5d^{5/2}$) are therefore forbidden at this band edge. The first transitions which we expect to be allowed appear at slightly higher energy for transitions into conduction states near Σ. This shifts the onset of core $5d^{5/2}$ transitions to the conduction band to higher energies by about 0.8 eV (for PbTe) and 1.0 eV(for PbSe) at 300°K with respect to the minimum energy at L. The first prominant peak at 20 eV for PbSe and 19.6 eV for PbTe originates from transitions from the $5d^{5/2}$ level into several closely spaced energy bands above the critical

point at Σ. The individual transitions can be identified with structure in the measured second derivative reflectivity spectrum as summarized in Table 3.

Transitions from the lower core d-levels ($5d^{3/2}$) start at about 20.6 eV for PbTe and 20.8 eV for PbSe. Unlike the $5d^{5/2}$ case these transitions involve states at the conduction band edge at L. Thus for transitions from the core $5d^{3/2}$ level the onset coincides with the band edge. Taking the spin orbit splitting for the lead core d-states to be 2.65 eV as determined by XPS and UPS measurements[21] and considering the shifts of 0.8 eV (PbTe) and 1 eV (PbSe) respectively for the onsets of the $5d^{5/2}$ transitions, we obtain an energy separation of the two thresholds for transitions from $5d^{5/2}$ and $5d^{3/2}$ levels of about 1.85 eV and 1.65 eV respectively in very good agreement with the reflectivity data. This result confirms the assumption, which is based on selection rules that the $5d^{5/2}$ transitions start at the Σ(6) band edge. Transitions from the $5d^{3/2}$ levels into the $6p^{3/2}$ conduction states are also allowed. They give rise to the shoulder or peak in the reflectivity at 22.8 eV for PbSe and 22.6 eV for PbTe. These structures however, are also due to transitions from $5d^{5/2}$ to higher conduction bands around Γ_8^-.

The relative heights of the two main peaks in the reflectivity can be explained by the different number of allowed transitions from the spin orbit split core d-levels:

there exist 12 transitions from $5d^{5/2}$ into $6p^{3/2}$ and 16 transitions from $5d^{3/2}$ into $6p^{3/2}$ and $6p^{1/2}$. This relative strength is not reproduced in our calculation which is probably due to the approximation made in using non-relativistic atomic radial wavefunctions.[4] We finally note that the total density of conduction states is nearly constant[1] thus indicating that the observed peak structures are dominated by matrix elements effects, i.e. the structure represents the strongly varying atomic character of conduction states.

Very interesting problems arise when attempting to locate the core d-levels on an absolute energy scale using X-ray (XPS) or ultraviolet (UPS) photoemission spectroscopy results.[21] The reference energy in these measurements is either taken to be the Fermi level or some significant structure in the valence bands. The combination of these data with low energy optical measurements allows independent determination (compared to synchrotron radiation measurements) of the energy separation between core-levels and known structure in the conduction bands. In particular we can use the $\Sigma(5)$ to $\Sigma(6)$ transition which has been observed at 300°K in the near infrared region at 1.24 eV for PbTe and 1.54 eV for PbSe.[5] The energy at 300°K of the $\Sigma(5)$ critical point falls at most 50 meV for PbTe[22] and 200 meV for PbSe[23] below the valence band edge. The lead $5d^{5/2}$ levels have been found from recent high resolution UPS measurements or previous XPS measurements[21] at 18.25 ± 0.1 eV below the valence band

edge for both lead salts. We thus obtain for the $5d^{5/2} \rightarrow \Sigma(6)$ threshold energies:

$$\Delta E \text{ (PbTe)} = 18.25 + 1.24 - 0.05 = 19.45 \ (\pm 0.1)\text{eV}$$

$$\Delta E \text{ (PbSe)} = 18.25 + 1.54 - 0.20 = 19.70 \ (\pm 0.1)\text{eV}$$

Comparing these energies to the threshold energies (ΔE(PbTe) = 18.65 eV and ΔE(PbSe) = 18.8 eV) measured in our experiment we find a characteristic shift in the reflectivity data of about 0.8 eV toward lower energies.

This shift is too large to be attributed to finite resolution effects or experimental errors. It therefore must arise from the difference in the nature of synchrotron radiation reflectivity measurements and photoemission spectroscopy. One possible explanation might invoke excitonic effects. Electron-hole interaction may play a role in synchrotron radiation reflectivity measurements but not in photoemission measurements. Excitonic effects with characteristic energies of the order of the observed shift (0.8 eV) would necessarily involve a large number of conduction bands, so that individual assignments to critical points and an interpretation in terms of classical excitons, would not be justified. Moreover, the comparison of the experimental and the calculated reflectivity seems to indicate that the electron-hole interaction results in a rather uniform shift of all structures with some deformation but without the appearance of new exciton-like peaks at lower energy. This deformation can be noticed e.g. for the main peak in the reflectivity which deviates from the calculated peak by

about 0.4 eV while the transition onsets are exactly aligned. The correctness of the conduction band structure in this range can be confirmed by inspecting the reflectivity measurements at low energies (see section III).

We now return to the results of the energy loss experiment[13] and compare these spectra with our calculated $\mathrm{Im}(1/\varepsilon)$ spectra (see Figs. 5 and 6 and Table 2). Again as in the comparison with the reflectivity data, the position in energy of the d-states has to be fit to experiment. In the reflectivity case a fit compatible with photoemission data could not be obtained. However in analyzing the energy loss experiments we find consistent results between the photoemission data and electron energy loss data. In other words the calculated $\mathrm{Im}(1/\varepsilon)$ using the energy positions of the d-levels based on photoemission results gives good agreement with electron energy loss data.

We do not encounter the difficulties in calculating the position of the d-state plasmon peaks in $\mathrm{Im}(1/t)$ that we had in determining the energy position of the main $\mathrm{Im}(1/\varepsilon)$ peak around 15 eV. In the latter case problems arose from the tail function used to extrapolate ε_2 to high energy. Since the peak around 6 eV (caused by p-like transitions) is also unaffected by the ε_2 extrapolation, we expect the energy separations between this peak and the d-peaks to be free from computational errors. We therefore have used these energy separations to analyze the electron energy

loss data. As stated above we did not observe (Table 2) the 0.9 eV shift found between the photoemission and reflectivity data.

The above assertion depends on the resolution of the structure in the electron energy loss experiment. The data presented in reference 13 do not include estimates of the errors involved in choosing the energy positions of the peaks. It is not unlikely that these errors can exceed the 0.9 eV shift discussed above. If, however, the observed difference between reflectivity and electron energy loss measurements is real, then the common practice of using the same dielectric function to analyze reflectivity and electron energy loss data is suspect. Further work, i.e. high resolution experiments and theoretical studies are necessary to clarify the situation.

VI. Conclusions

We have presented in this paper calculations related to several optical measurements of PbSe and PbTe which are based on band structure models developed in paper I. First the calculated spectra are compared to modulated reflectivity measurements for energies up to 6 eV. Most of the empirical parameters in the band structure calculations were adjusted to fit these data with high precision.

The real part of the refractive index which has been calculated with and without the use of orthogonalized wave functions was compared to experiment for low energies.

The good agreement between theory and experiment for the index is considered to be a strong indication of the quality of the calculated wavefunctions. Several peaks in the calculated imaginary part of $1/\varepsilon$ are attributed to observed plasma oscillations of different "groups" of electrons.

Finally optical properties in the energy range from 18 to 26 eV arising from transitions from the cation core d-levels into conduction states are investigated theoretically and compared to recent synchrotron radiation reflectivity measurements, to energy loss experiments and to XPS and UPS photoemission data.

References

* Supported in part by the National Science Foundation Grant GH 35688.

† On leave from University of Paris VI, France on NATO fellowship. Permanent address: Laboratoire de physique des solides, Université Paris VI, 4 place Jussieu, 75 Paris 5°, France.

‡ Swiss National Science Foundation fellow.

1. G. Martinez, M. Schlüter and M. L. Cohen, to be published, hereafter referred to as paper I.

2. G. Gilat and G. Dolling, Phys. Letters 8, 304 (1964).

3. G. Martinez, M. Schlüter, M. L. Cohen, R. Pinchaux, P. Thiry, D. Dagneaux and Y. Petroff, to be published.

4. F. Hermann, S. Skillman in Atomic structure calculations, Prentice-Hall, Inc., Englewood Cliffs, N.J. 1963.

5. M. Cardona and D. L. Greenaway, Phys. Rev. 133, A1685 (1964). V. V. Sobolev and V. I. Donetskik, Soviet Physics Solid State 12, 1408 (1970).

6. S. E. Kohn, P. Y. Yu , Y. Petroff, Y. R. Shen, Y. Tsang and M. L. Cohen, Phys. Rev. B8, 1477 (1973).

7. D. L. Mitchell, E. D. Palick and J. N. Zemel. Proceedings of the 7th International Conference on the Physics of Semiconductors, p. 325, Dunod, Paris (1964).

8. T. C. Harman, A. R. Calawa, I. Melngailis and J. O. Dimmock, Appl. Phys. Letters 14, 333 (1969).

9. D. E. Aspnes and M. Cardona, Phys. Rev. 173, 714 (1968).

10. J. R. Chelikowsky and M. L. Cohen, Phys. Rev. Letters 31, 1582 (1973).

11. A. Baldereschi, Phys. Rev. B7, 5212 (1973).

12. T. K. Bergstresser and G. W. Rubloff, Phys. Rev. Letters 30, 794 (1973).

13. B. Lahaye, F. Pradal and C. Gout, J. de Physique C4, 137 (1968).

14. P. Nozieres and D. Pines, Phys. Rev. 113, 1254 (1959).

15. H. R. Philipp and H. Ehrenreich, Phys. Rev. 129, 1550 (1953).

16. G. Martinez, M. Schlüter and M. L. Cohen, to be published.

17. J. N. Zemel, J. D. Jensen and R. B. Schoolar, Phys. Rev. 140, A330 (1965).

18. N. Piccioli, J. N. Besson and M. Balkanski, J. Phys. Chem. Solids 35, 971 (1974).

19. M. Cardona, C. M. Denchina, E. E. Koch and P. Y. Yu, Phys. Stat. Solidi b58, 127 (1973).

20. J. Y. Leloup, B. Sapoval and G. Martinez, Phys. Rev. 7B, 5276 (1973).

21. F. R. McFeely, S. Kowalczyk, L. Ley, R. A. Pollak and D. A. Shirley, Phys. Rev. B7, 5228 (1973); and D. Eastman, private communication.

22. R. N. Tauber, A. A. Machonis and I. B. Cadoff, J. Appl. Phys. 37, 4855 (1966).

23. A. A. Andreev, J. de Physique C4, 50 (1968).

Table Captions

Table 1. Comparison between calculated structure in the reflectivity (R) and its first derivative (R') and experimental reflectivity and absorption (A) and emission (E) measurements for PbTe (a) and PbSe (b). The calculations are done for 0°K; the temperatures for the various experiments are indicated. The important transitions giving rise to structure are identified and their locations in k-space are given. The point P has the coordinates (0.625,0.46,0). The table corresponds to Figs. 1, 3 and 4.

Table 2. Comparison between experimental energy loss data and calculated structure in the imaginary part of $1/\varepsilon$. The calculations are done with and without OPW matrix element corrections. The origins of the various peaks are also indicated. The table corresponds to Figs. 5 and 6.

Table 3. Assignment of minima in the experimental second derivative of the reflectivity to individual core-conduction band transitions. The energy zeros are taken at the respective reflectivity thresholds at $\Sigma(6)$ corresponding to 18.65 eV for PbTe and 18.8 eV for PbSe. Σ_1', Δ' and Δ'' stand for regions in K-space around Σ and Δ respectively. P is the critical point with the coordinates (0.625,0.46,0) which also gives rise to the highest peak in ε_2 (see Table 1).

Table 1

(a) PbTe

Type of Experiment, reference and temperature	Experimental energies	Theoretical energies	Critical point symmetry	Transition
$A^{(7)}$ 4°K	0.190	0.189	M_0	L(5-6)
$R^{(5)}$ 300°K	1.24	1.20	M_1	Σ(5-6)
$R'^{(6)}$ 4°K	2.16	2.10	M_1	Σ(4-6)
"	2.25	2.21	volume	P(5-6)
"	2.36	2.46	M_1-M_0	Σ(5-7),Δ(5-6)
"	2.56	2.70	volume	around P(5-6)
"	3.47	3.40	M_1	Σ(4-7)
"	4.83	4.90	volume	around Λ(3-8)
"	5.90	6.00	M_1	X(5-6)
$R^{(5)}$ 300°K	7.3	7.3	M_0	[Σ(4-10) K(5-8)
$R^{(5)}$ 300°K	7.8	8.05	volume	[Λ near Γ(3-10) Σ(4-10)
$R^{(5)}$ 300°K	11.2	11.15	M_2	Σ(5-12)
$R^{(5)}$ 300°K	12.5	12.5±0.2	volume	Σ near K(3-11)

(b) PbSe

$A^{(7)}$ 4°K	0.160]	0.157	M_0	L(5-6)
$E^{(8)}$ 4°K	0.150			
$R^{(5)}$ 300°K	1.54-1.59	1.48	M_1	Σ(5-6)

$R'^{(6)}$	4°K	1.97]	2.0	volume	around Λ(5-6)
	"	2.20]			
	"	2.65	2.75	volume	P(5-6)
	"	2.84	3.00	M_1-M_0	Σ(4-6),Δ(5-6)
	"	3.12	3.27	volume	around Σ(4-6)
	"	4.47	4.35	M_1	Σ(4-7),L(3-8)
	"	5.52	[5.44 5.63	volume M_1	around Λ(3-8) Σ(5-8)
$R^{(5)}$	300°K	6.3	6.50	volume	Δ near X(5-6)
$R^{(5)}$	300°K	7.1	7.3	volume	Δ near Γ(3-7)
$R^{(5)}$	300°K	7.7	7.83	volume	Δ near Γ(5-10)
$R^{(5)}$	300°K	8.8]			
$R^{(5)}$	300°K	9.1]	8.90	volume	Σ near Γ(4,5-10)
$R^{(5)}$	300°K	12.5	12.3±0.3	volume	around Σ(5-12)

Table 2

	Experimental[13] peaks (eV)	Calculated with pseudo matrix elements	Calculated with OPW matrix elements	Origin
	5.7	5.6	5.65	p valence states
	9.7	9.5	9.6	s lead valence states
PbTe	15	13.8	15.5	all valence states
	20.7	20.5	20.5	$5d^{5/2}$ lead states
	22.7	22.6	22.6	5d lead states
	7.0	6.1	6.2	p valence states
	11.0	--	--	s lead valence states
PbSe	15.8	14.0	15.4	all valence states
	20.5	20.6	20.6	$5d^{5/2}$ lead states
	22.8	23.0	23.0	5d lead states

Table 3

PbSe			PbTe		
Transition	Theory	exp	Transition	Theory	exp
$d^{5/2} \rightarrow \Sigma(6)$	0	0	$d^{5/2} \rightarrow \Sigma(6)$	0	0
$d^{5/2} \rightarrow \Lambda(7)$	0.70	0.68	$d^{5/2} \rightarrow \begin{cases}\Sigma(7) \\ \Sigma'(7)\end{cases}$	0.70 1.20	0.92
$d^{5/2} \rightarrow \begin{cases}\Sigma(7) \\ \Sigma'(7)\end{cases}$	1.20	1.24	$d^{5/2} \rightarrow \Lambda(7,8)$	1.55	1.58
$d^{3/2} \rightarrow L(6)$	1.75	1.85	$d^{3/2} \rightarrow L(6)$	1.97	1.99
$d^{3/2} \rightarrow \Sigma(6)$	2.55	2.60	$d^{3/2} \rightarrow \Sigma(6)$	2.55	2.58
$d^{3/2} \rightarrow \begin{cases}\Delta(6) \\ P(6)\end{cases}$	3.05 3.45	2.82	$d^{3/2} \rightarrow \begin{cases}\Delta(6) \\ P(6)\end{cases}$	3.15	2.85
$d^{3/2} \rightarrow \begin{cases}\Sigma'(6) \\ \Lambda(6)\end{cases}$	3.95±0.1	4.02	$d^{3/2} \rightarrow \begin{cases}\Sigma'(6) \\ \Lambda(6)\end{cases}$	3.65	3.46
$d^{5/2} \rightarrow \Delta'(6)$	4.55		$d^{3/2} \rightarrow \Delta'(6)$	4.05	3.98
$d^{5/2} \rightarrow \Gamma(10)$ $d^{3/2} \rightarrow \Gamma(6)$	4.85	4.57	$d^{3/2} \rightarrow \Gamma(6)$	4.50	4.36
--	--	5.62	$d^{3/2} \rightarrow \Delta''(6)$	5.65	5.30±0.2
$d^{3/2} \rightarrow \Delta''(7)$	6.45±0.2	6.33±0.1			

Figure Captions

Figure 1. Experimental modulated reflectivity of (a) PbTe and (b) PbSe as obtained from Ref. 6. The theoretical curve is the calculated first derivative of reflectivity.

Figure 2. Band structure of PbTe as calculated in Ref. 1.

Figure 3. Imaginary part of the dielectric function $\varepsilon_2(\omega)$ for PbTe calculated with (full line) and without (dashed line) OPW matrix element corrections. Also indicated is the calculated reflectivity (with OPW matrix element corrections) (full line) together with the experimental reflectivity of Ref. 6 (dotted line).

Figure 4. Imaginary part of the dielectric function for PbSe. See caption for Fig. 3.

Figure 5. Imaginary part of $1/\varepsilon$ for PbSe calculated with (full line) and without (dashed line) OPW matrix element corrections. The core- to conduction band transitions above about 18 eV are always calculated with OPW matrix element corrections.

Figure 6. Imaginary part of $1/\varepsilon$ for PbTe. See caption for Fig. 5.

Figure 7. Index of refraction for PbTe obtained experimentally in Ref. 17 (dashed line) and in Ref. 18 (dotted line). For PbSe only one experiment[17] is available. The data are compared to calculated spectra using pseudo wavefunctions and OPW's respectively. The calculations are done for 0°K while the experiments were done at

80°K[17] and 25°K[18] respectively with doped samples. This accounts for the shift in energy of the experimental peaks with respect to theory.

Figure 8. Reflectivity (a) and second derivative spectrum for measured reflectivity (b) for PbSe. The theoretical reflectivity curve is indicated by the broken line. The assignments in part (b) are explained in Table 3.

Figure 9. Reflectivity and second derivative spectrum for PbTe. See caption for Fig. 8.

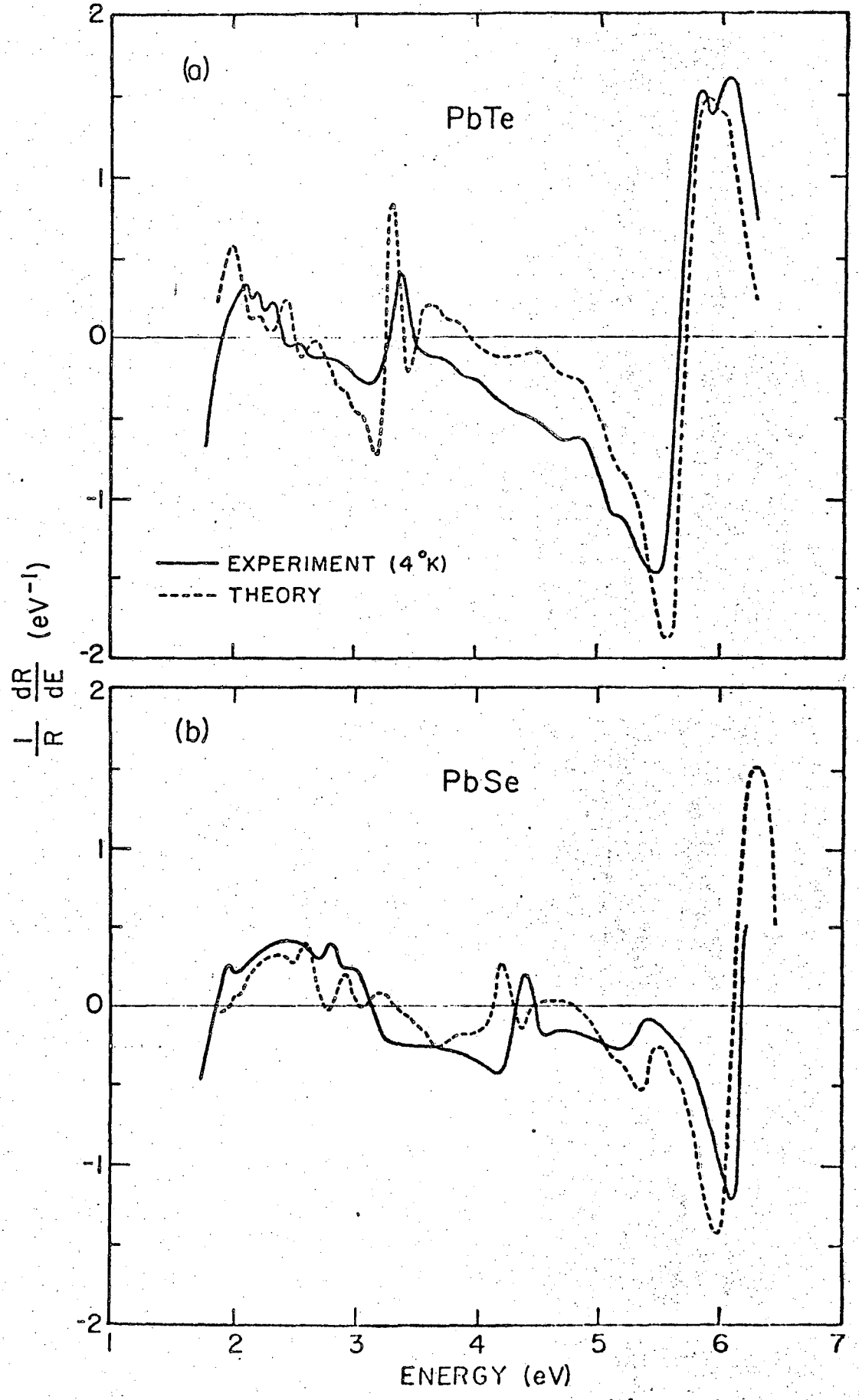

Figure 1

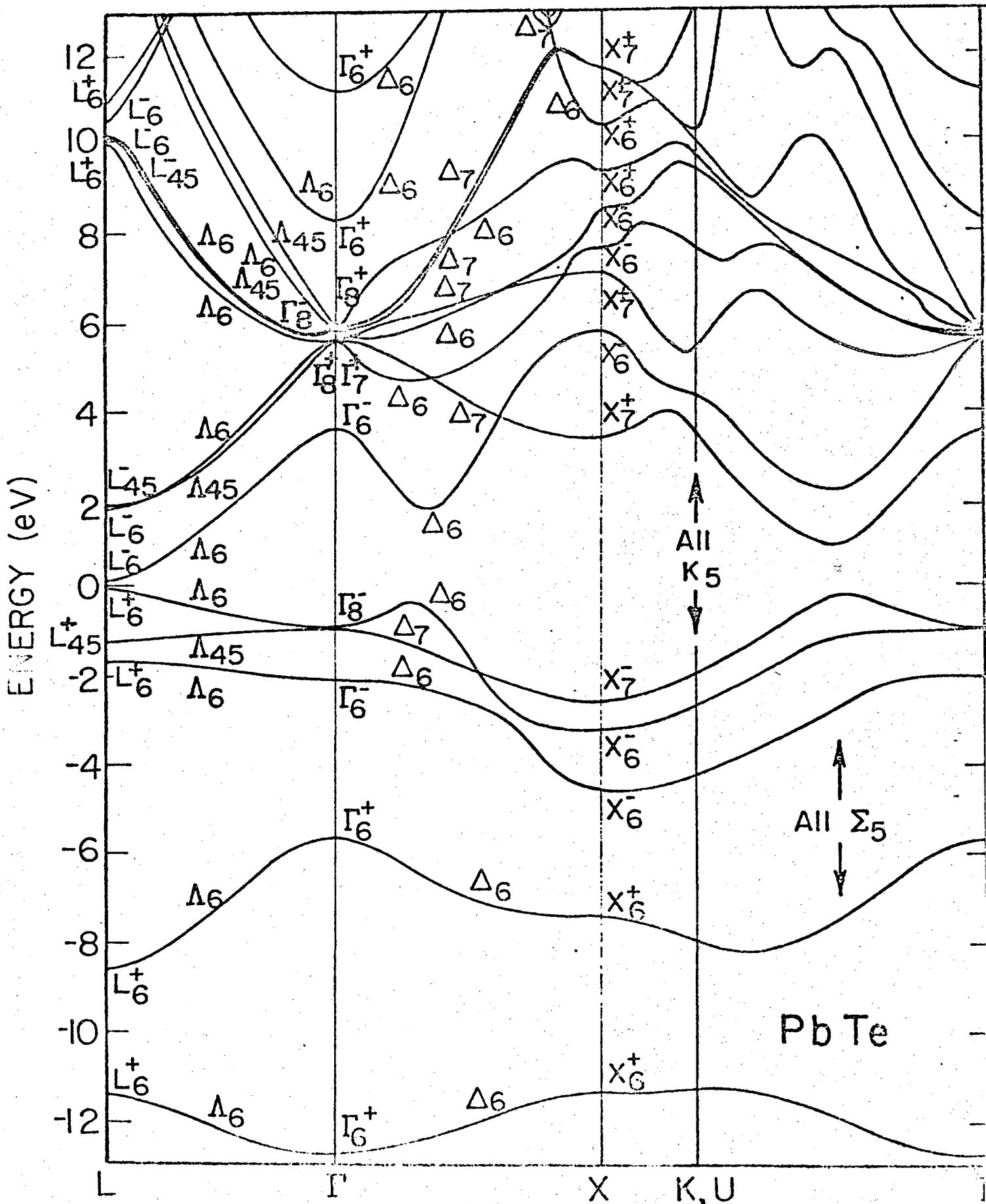

Figure 2

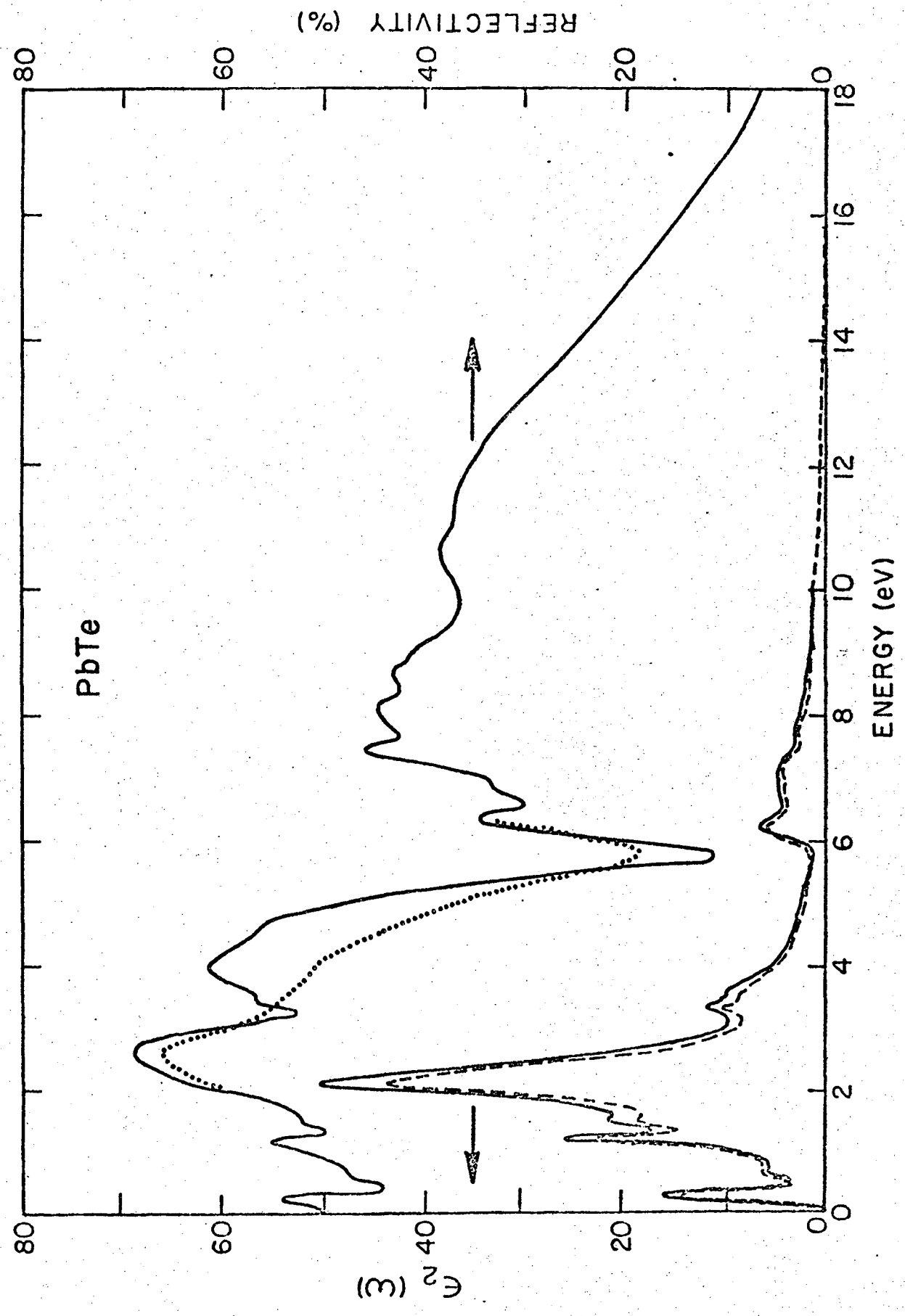

Figure 3

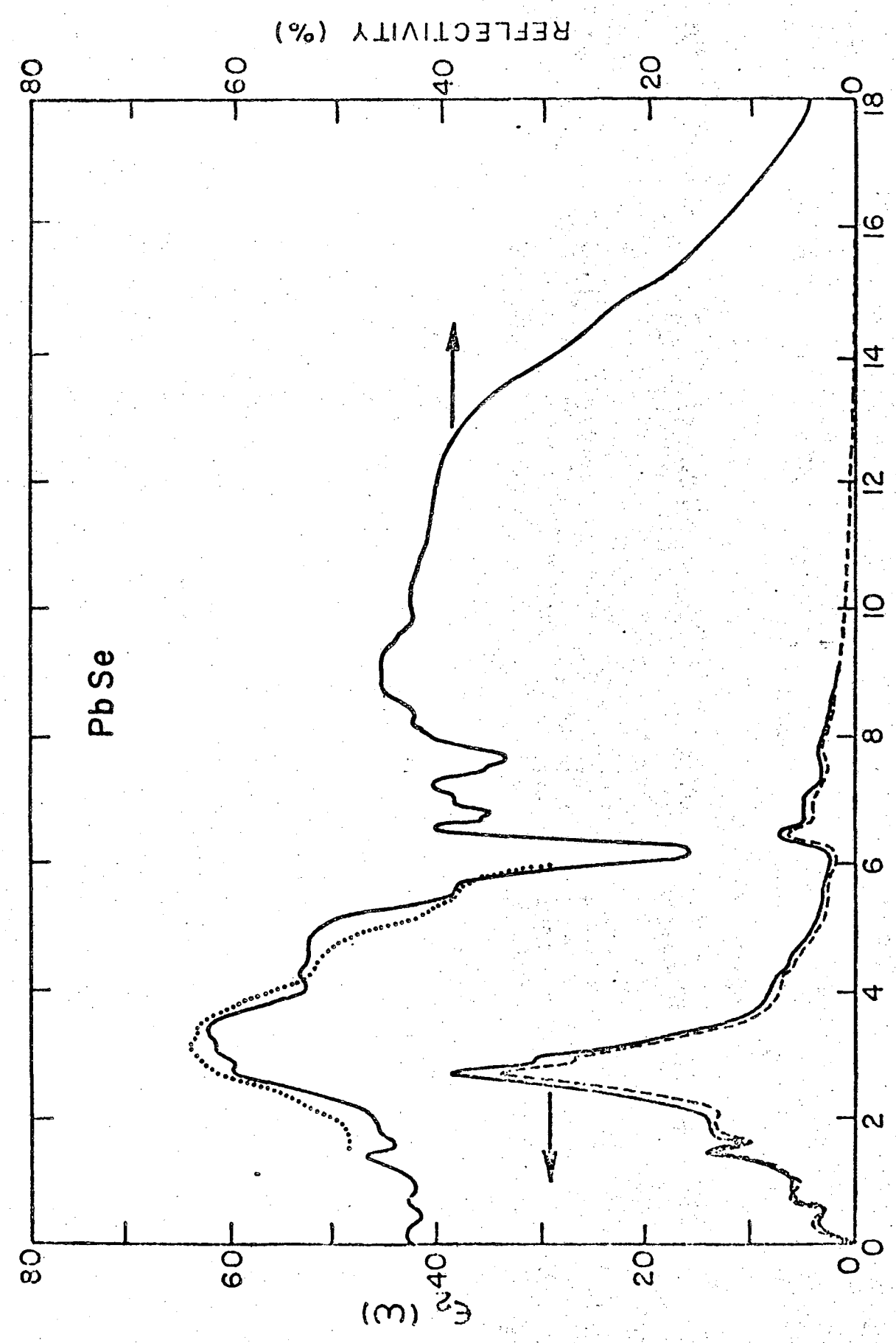
REFLECTIVITY (%)
80
60
40
20
0
PbSe
ENERGY (eV)
0
2
4
6
8
10
12
14
16
18
(3) ω

Figure 4

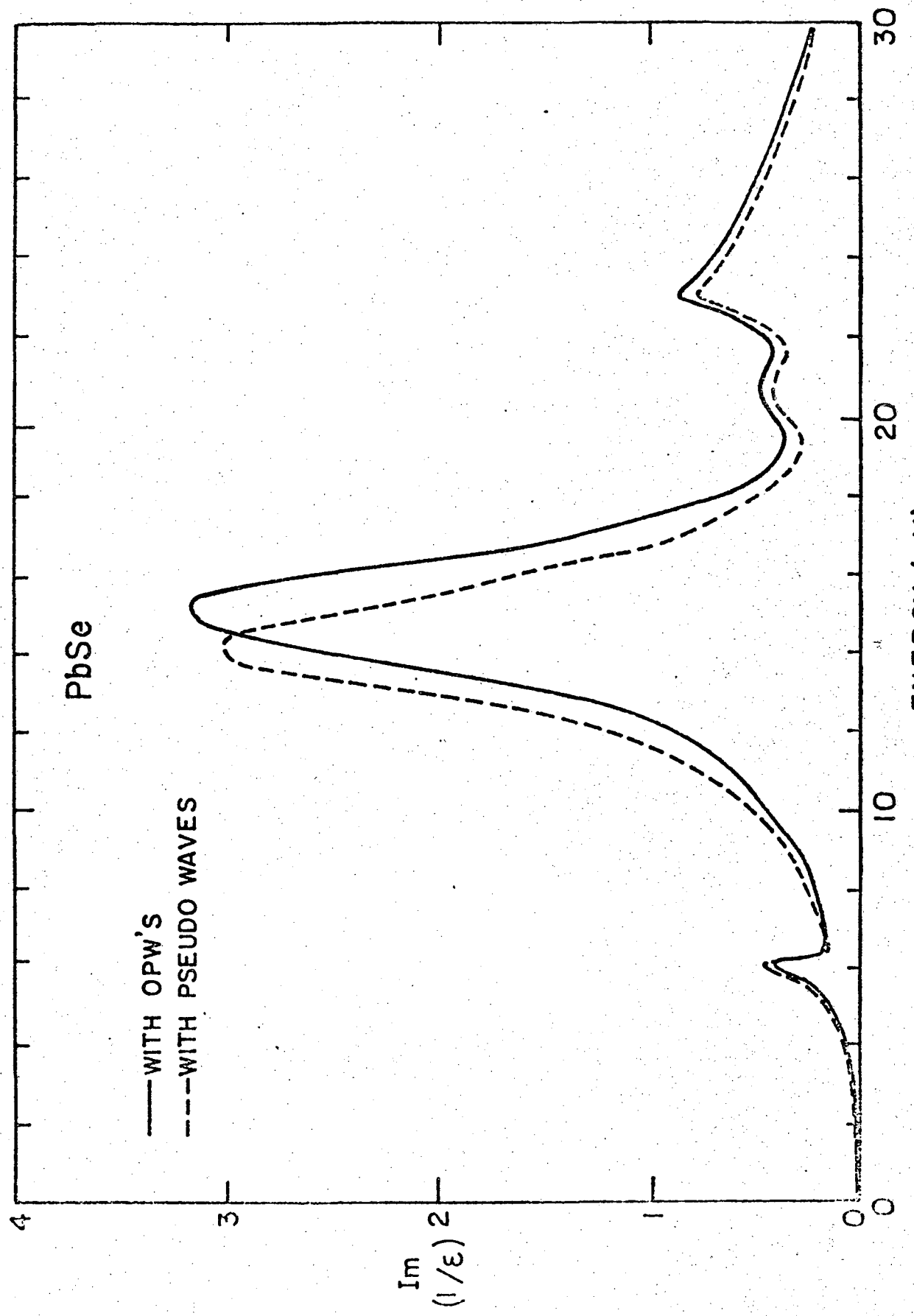

Figure 5

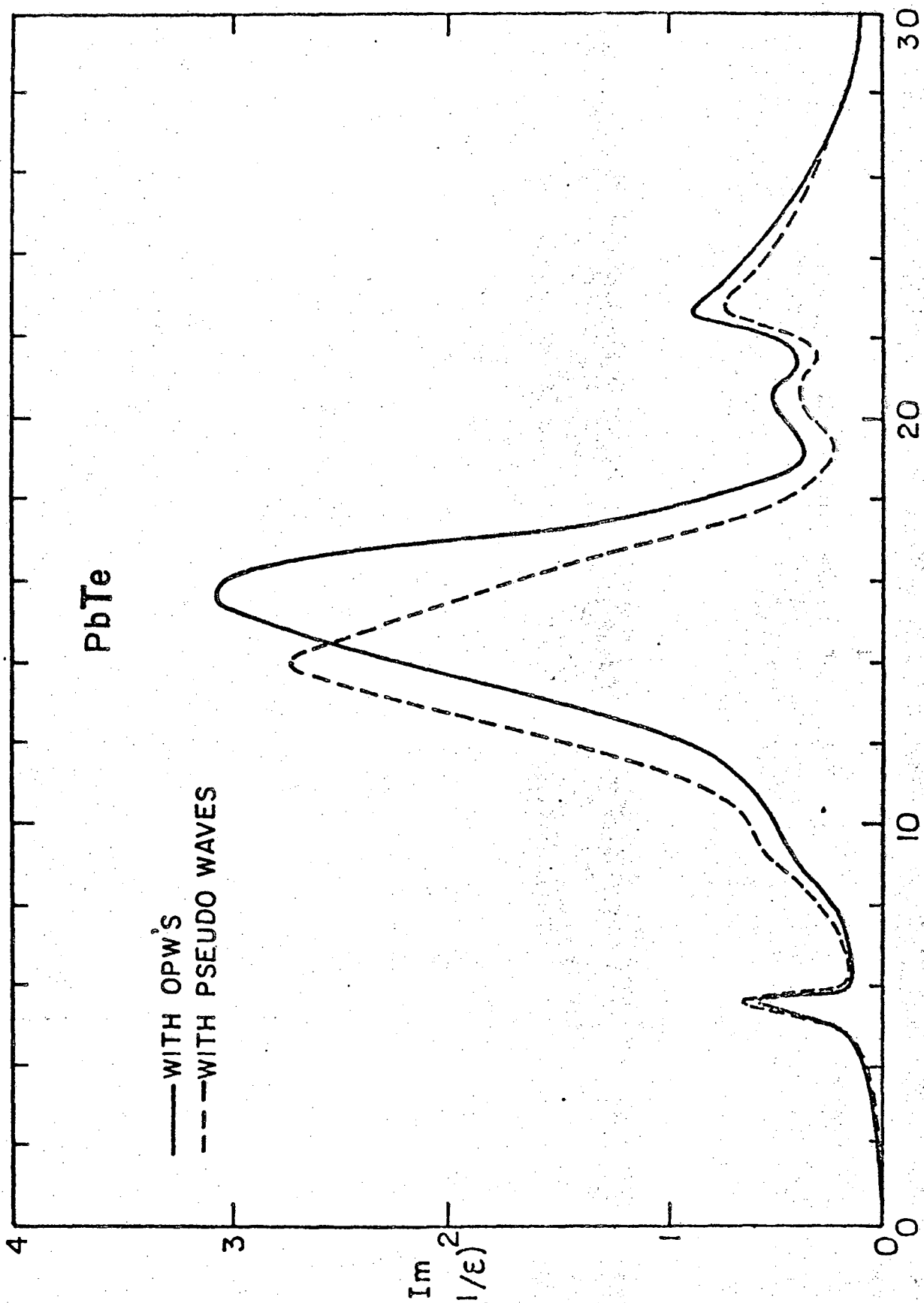
PbTe
WITH OPW'S
WITH PSEUDO WAVES
Im $(1/\varepsilon)^2$
ENERGY (eV)
0
1
3
4
10
20
30

Figure 6

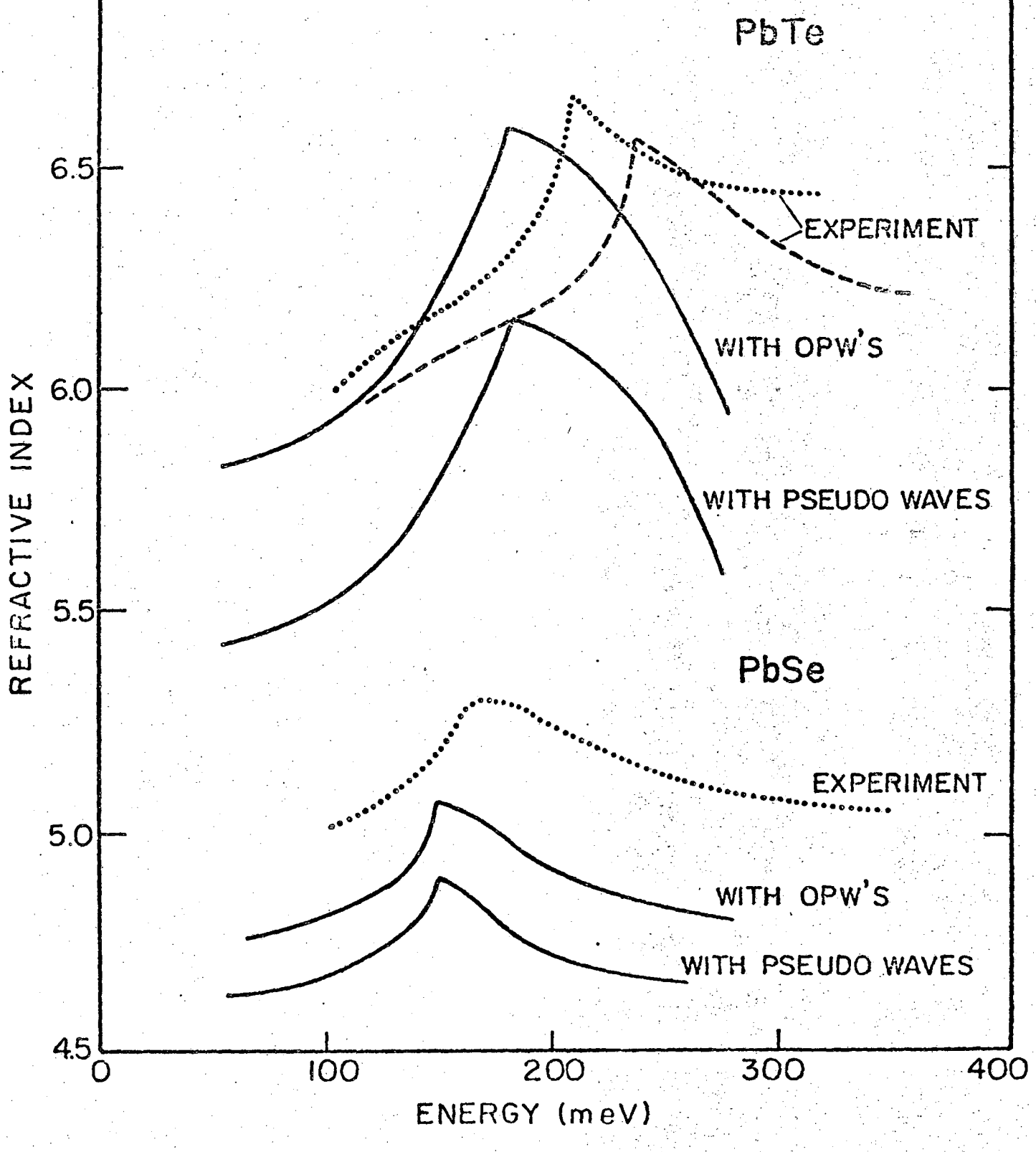

Figure 7

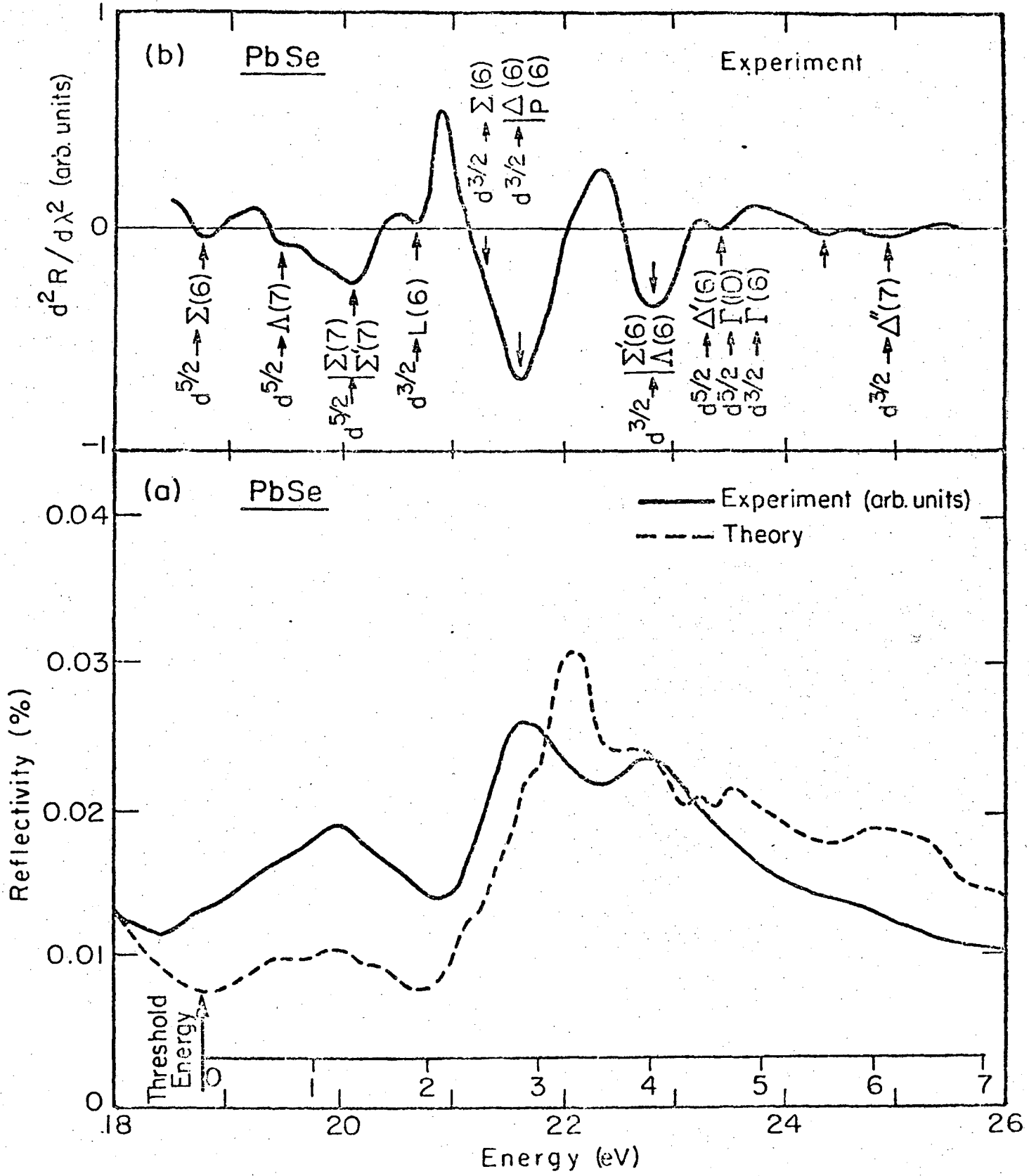
(b) PbSe
Experiment
$d^2R/d\lambda^2$ (arb. units)
$d^{5/2} \rightarrow \Sigma(6)$
$d^{5/2} \rightarrow \Lambda(7)$
$d^{5/2} \rightarrow \Sigma(7), \Sigma'(7)$
$d^{3/2} \rightarrow L(6)$
$d^{3/2} \rightarrow \Sigma(6)$
$d^{3/2} \rightarrow \Delta(6), P(6)$
$d^{3/2} \rightarrow \Sigma'(6), \Lambda(6)$
$d^{5/2} \rightarrow \Delta'(6)$
$d^{5/2} \rightarrow \Gamma(10)$
$d^{3/2} \rightarrow \Gamma(6)$
$d^{3/2} \rightarrow \Delta''(7)$
(a) PbSe
Experiment (arb. units)
Theory
Reflectivity (%)
Threshold Energy
Energy (eV)
XBL 748-6989

Figure 8

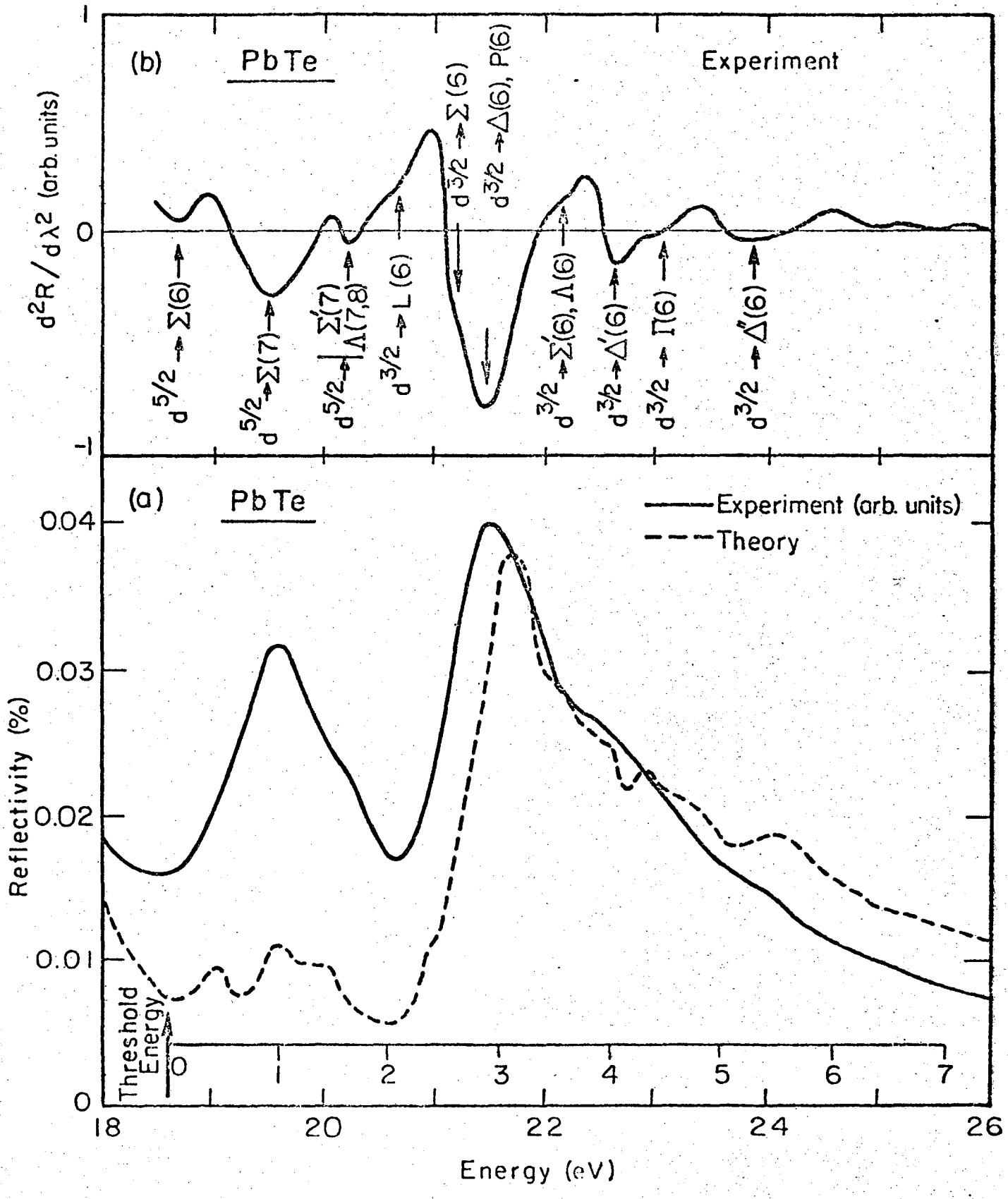

Figure 9

XBL748-6988

TECHNICAL INFORMATION DIVISION
LAWRENCE BERKELEY LABORATORY
UNIVERSITY OF CALIFORNIA
BERKELEY, CALIFORNIA 94720